S1. Supplementary material

This document provides additional images, tables, and text. All references to tables and figures in the main manuscript are given in plain numbers, while tables and figures in the supplement are indicated by a prefix "S". The supplement is structured analogously to the manuscript. I.e., additional material to section 2.3 can be found in section S2.3 of the supplement.

S2. Methods

S2.1 Terminology

Abbreviations are defined in the main manuscript (Table 2). All column densities are given in column density units of 1 CDU=10^{15} molec cm^{-2}.

STS performance is analyzed based on tropospheric residues (TR) (Eq. 1); tropospheric VCDs are generally higher than TR by the ratio $A_{\mathrm{strat}}/A_{\mathrm{trop}}$. Figure S1 displays the monthly mean of this ratio of AMFs, as provided in the NASA product, for cloud free conditions.

Within the discussion of the MPI-C STS for SCIAMACHY based on LNM (Beirle et al., 2010), tropospheric SCDs (TSCDs) have been analyzed. For OMI, however, viewing angle dependencies would dominate daily maps of TSCDs due to the far larger range of viewing angles of OMI compared to SCIAMACHY. In this study, we thus focus on TR, i.e. we applied stratospheric AMFs in order to eliminate the viewing angle dependencies of TSCDs.

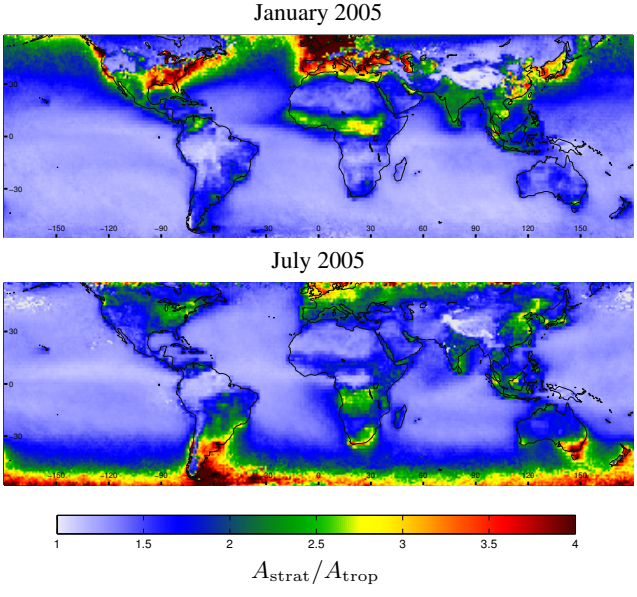

Fig. S 1. Ratio of monthly mean stratospheric and tropospheric AMFs as provided by NASA for cloud free observations (CRF<0.3) for January (top) and July (bottom) 2005. On average, cloud free TVCDs are higher than TRs by this ratio (Eq. 2).

S2.2 Weighting factors

S2.2.1 Pollution weight

If the stratospheric NO_2 is estimated from total column density measurements, regions with tropospheric pollution have to be excluded. Thus, we assign potentially polluted satellite pixels a pollution weight $w_{\mathrm{pol}}<1$ based on our a-priori knowledge of tropospheric NO_2. For this purpose we use a climatology of tropospheric NO_2 column densities from SCIAMACHY measurements 2003-2011 (Beirle and Wagner, 2012) shown in Fig. S2a. Pollution weights are defined based on a pollution proxy which is derived from the NO_2 climatology by the following steps:

1. Grid pixels with a mean TVCD below 1 CDU are removed (Fig. S2b).
2. The resulting clipped climatology is smoothed by convolution with a 2D-Gaussian with $\sigma = 2^\circ$ (Fig. S2c).
3. For the pollution proxy P, values between 0 and 1 CDU are set to 1 CDU. By this operation, a "safety margin" of *potentially* polluted areas is created (Fig. S2d).

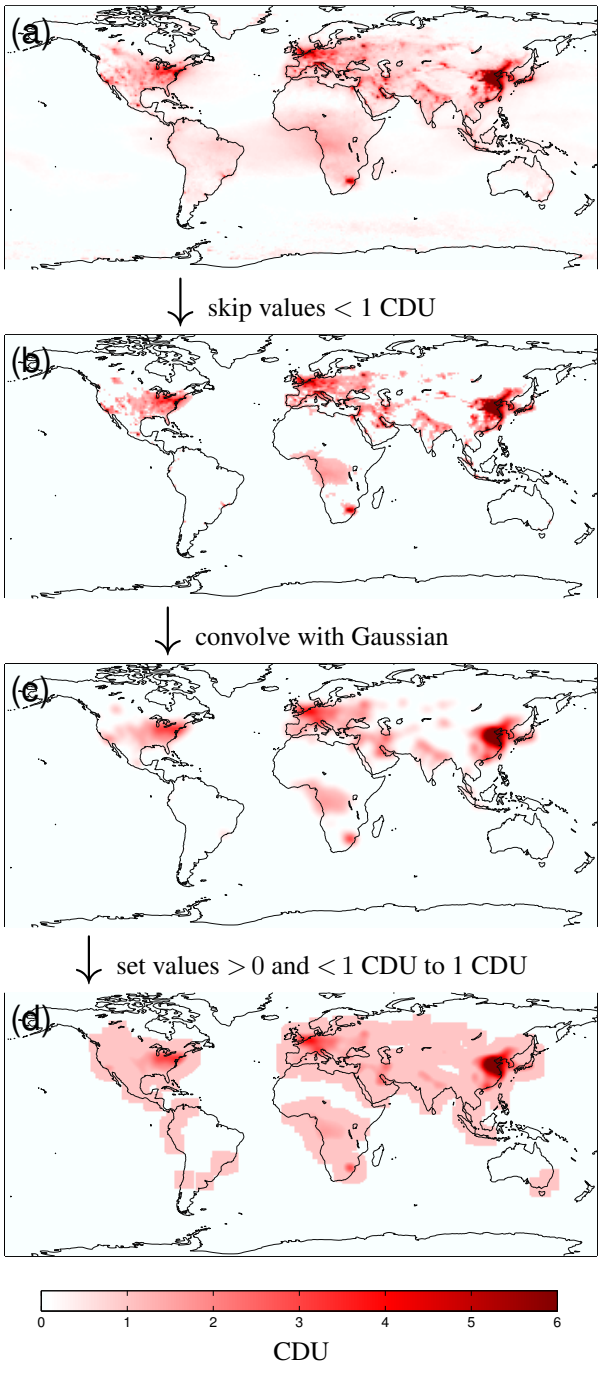

Fig. S 2. Stages of the calculation of the pollution proxy P: The tropospheric NO_2 climatology (a) is clipped to values >1 CDU (b), convolved with a Gaussian (c), and extended in space by setting values between 0 and 1 CDU to a minimum of 1 CDU (d).

S2.3 Weighted convolution

We illustrate the procedure of weighted convolution, as explained in Section 2.3 of the manuscript and described by eqs. (7)-(12), by a simple, constructed example on a 10×1 grid.

Table S1 lists the values for V^* and their respective weights. Pixels 1-3 and 9-10 are free of tropospheric pollution, while pixels 5-8 are exposed to regular tropospheric pollution, causing low values for w_{pol}. Two observations were made under cloudy conditions, causing a cloud weight >1. Figure S3 displays the respective individual VCDs v_{ik} (with their net weights shown by color) and the stratospheric estimate $\overline{V}$ resulting from weighted convolution.

Table S 1. NO_2 VCDs and weighting factors for the constructed example for illustration of weighted convolution.

i	k	v_{ik}	w_{pol}	w_{cld}	w
1	1	1.1	1	1	1
2	1	1.15	1	1	1
	2	0.95	1	20	20
3	1	1.1	1	1	1
4					
5	1	1.5	0.15	1	0.15
6	1	2	0.05	1	0.05
	2	1.1	0.05	50	2.5
7	1	3.5	0.025	1	0.025
8	1	2	0.05	1	0.05
9	1	1.1	0.1	1	0.1
10	1	1.05	1	1	1

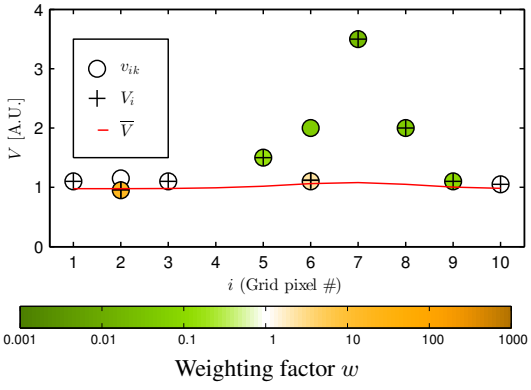

Fig. S 3. Illustration of weighted convolution for the constructed VCDs listed in table 1. Weighting factors are color coded. Circles represent the individual V^* for each satellite pixel. The weighted mean VCD in each grid pixel (eq. 9) is indicated by a "+". In cases of multiple satellite pixels per grid (i=2,6), the weighted mean is dominated by the clouded satellite pixel due to the heigh weighting factor. The finally resulting stratospheric pattern $\overline{V}$ is shown in red.

Two convolution kernels G^{pol} and G^{eq}, as defined in Eq. 15, are used in STREAM, matching the different needs for high versus low latitudes, respectively. G^{pol} and G^{eq} are displayed in Fig. S4.

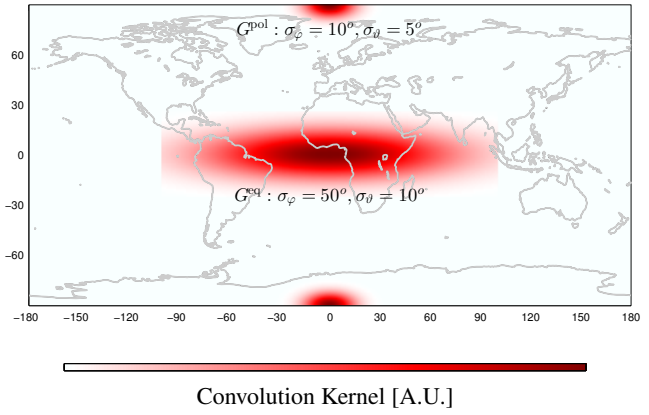

Fig. S 4. Illustration of the convolution kernels used for weighted convolution at the poles and at the equator, respectively. G^{eq} is clipped to $\pm 100^\circ$, i.e. $\pm 2\sigma_\varphi$, to keep computation time low. Global convolution results from the weighted mean of both kernels according to Eq. 15.

In STREAM default set-up, the overall latitudinal dependency of V^* is estimated over the Pacific, removed before the weighted convolution, and added again thereafter. This procedure avoids artefacts of latitudinal convolution in case of gradients on spatial scales of σ_ϑ or smaller. Figure S5 illustrates this effect; the impact of the latitude correction on the resulting TR will be shown in detail below (section S5.3.1).

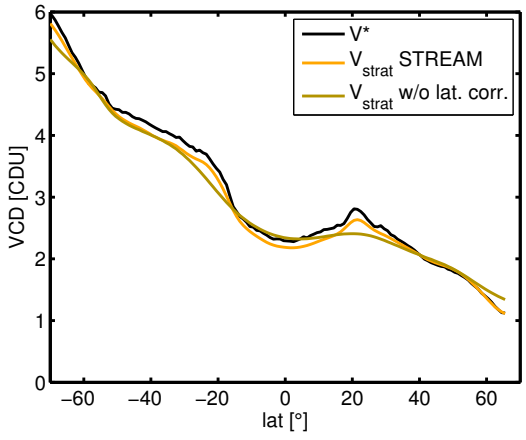

Fig. S 5. Mean total column V^* and stratospheric estimates as function of latitude from STREAM with and without initial latitude correction over the Pacific for OMI data on 1 January OMI.

S4 Algorithm performance

S4.1 STREAM versus RSM for OMI

Figure S6 provides information on the definition of percentile bars, and figure S7 shows the definition of the regions used for the regional statistical analysis in Figs.6-8, 12, 14 and 16, and several diagrams in the supplement.

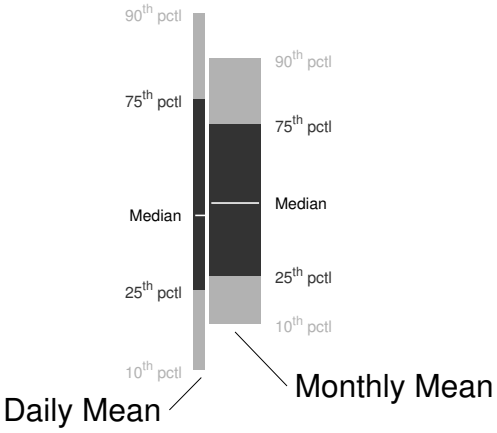

Fig. S 6. Illustration of the meaning of percentile bars used in diagrams on regional statistics of T^*. Light and dark bars reflect the 10^{th}-90^{th} and 25^{th}-75^{th} percentiles, respectively. The median is indicated in white. The narrow and wide bars show the statistics for the first day of the month and the monthly mean, respectively.

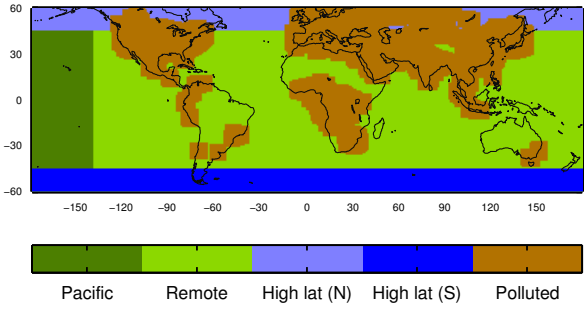

Fig. S 7. Definition of the regions used for the calculation of the statistics of T^*. Note that in the diagram "high latitudes" always refers to the repective winter hemisphere.

S4.2 Impact of a-priori settings

S4.2.1 Impact of cloud weight w_{cld}

Figures S8 and S9 display the TR resulting from STREAM for w_{cld} switched off and increased by a factor of 10, respectively, for OMI in 2005. Figure S10 displays the respective TR if low clouds are also considered for the calculation of w_{TR} (by setting $w_{\mathrm{P}} = 1$ for $p > p_{\mathrm{ref}}$ in Eq. 6(c)). The respective regional statistics of T^* are shown in Fig. S11.

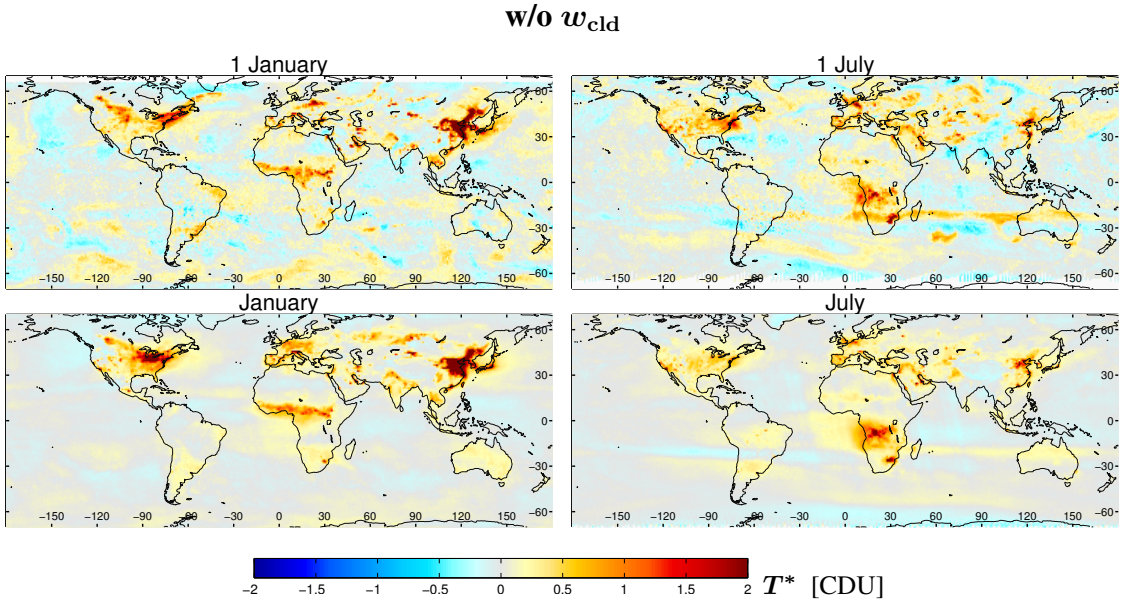

Fig. S 8. OMI tropospheric residues T^* based on STREAM for January (left) and July (right) 2005 for the first day of the month (top) and the monthly mean (bottom) without applying w_{cld}.

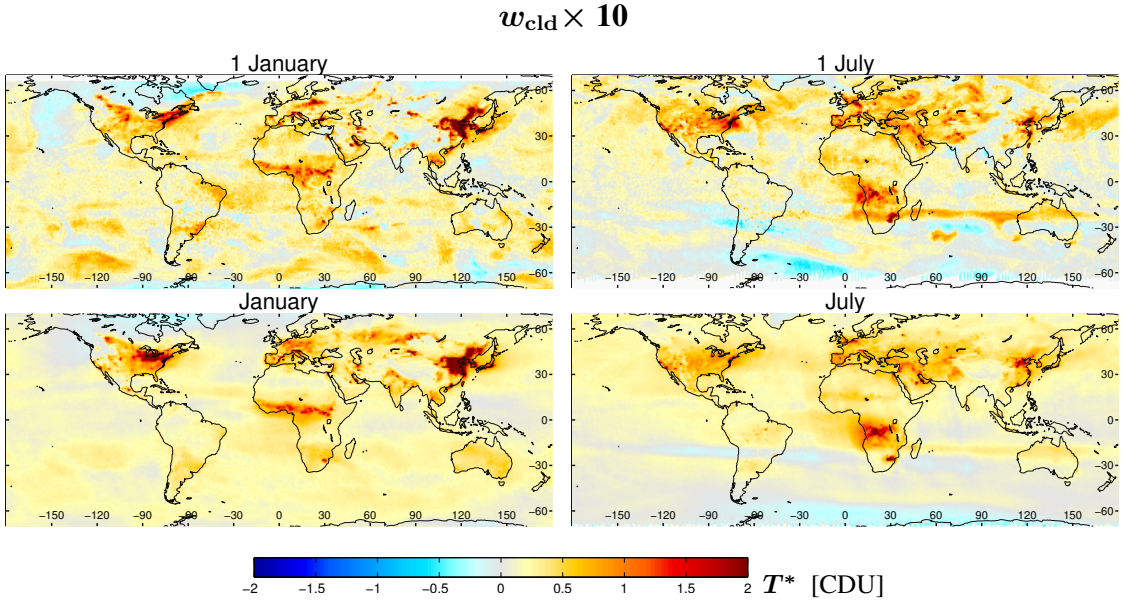

Fig. S 9. OMI tropospheric residues T^* based on STREAM for January (left) and July (right) 2005 for the first day of the month (top) and the monthly mean (bottom) for high w_{cld} ($\times 10$ compared to baseline).

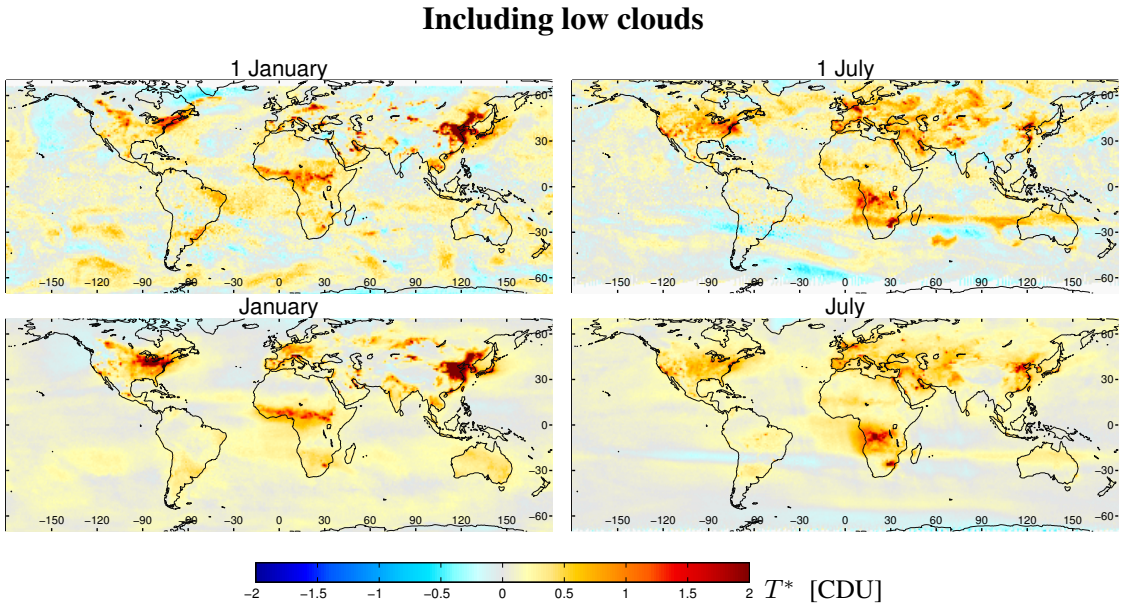

Fig. S 10. OMI tropospheric residues T^* based on STREAM for January (left) and July (right) 2005 for the first day of the month (top) and the monthly mean (bottom) for w_{cld} based on clouds of medium or low altitude.

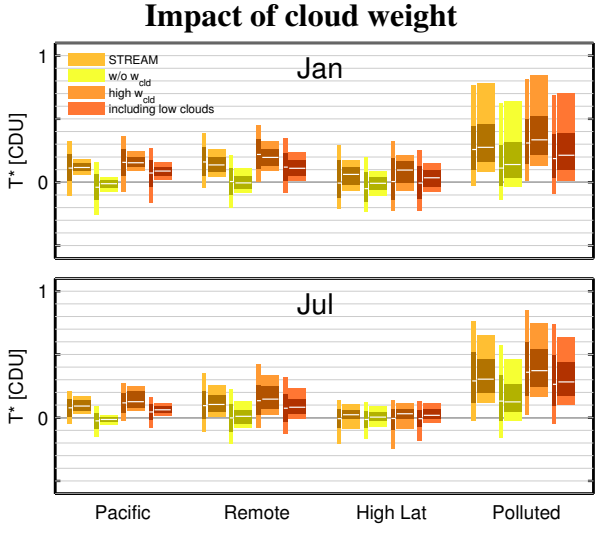

Fig. S 11. Regional statistics of OMI tropospheric residues T^* from STREAM for different settings of w_{cld}. Light and dark bars reflect the 10-90$^{\mathrm{th}}$ and 25-75$^{\mathrm{th}}$ percentiles, respectively. The median is indicated in white. Narrow bars show the statistics for the first day of the month, wide bars those of the monthly means (see also Fig. S6 for illustration). The regions are defined in Fig. S7. "High latitudes" refer to the respective hemispheric winter only.

S4.2.2 Impact of convolution kernel

Figures S12 and 13 display the TR resulting from STREAM for the convolution kernels G^{pol} and G^{eq} applied globally, respectively, for OMI in 2005.
The respective regional statistics of T^* are shown in Fig. S14.

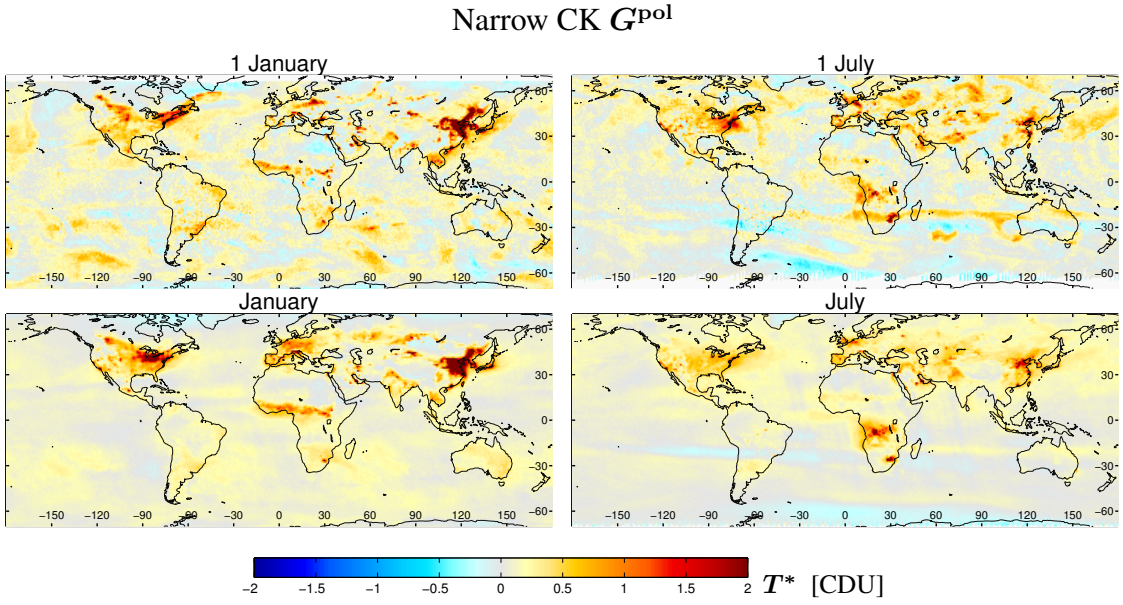

Fig. S 12. OMI tropospheric residues T^* based on STREAM for January (left) and July (right) 2005 for the first day of the month (top) and the monthly mean (bottom) resulting from weighted convolution using G^{pol}.

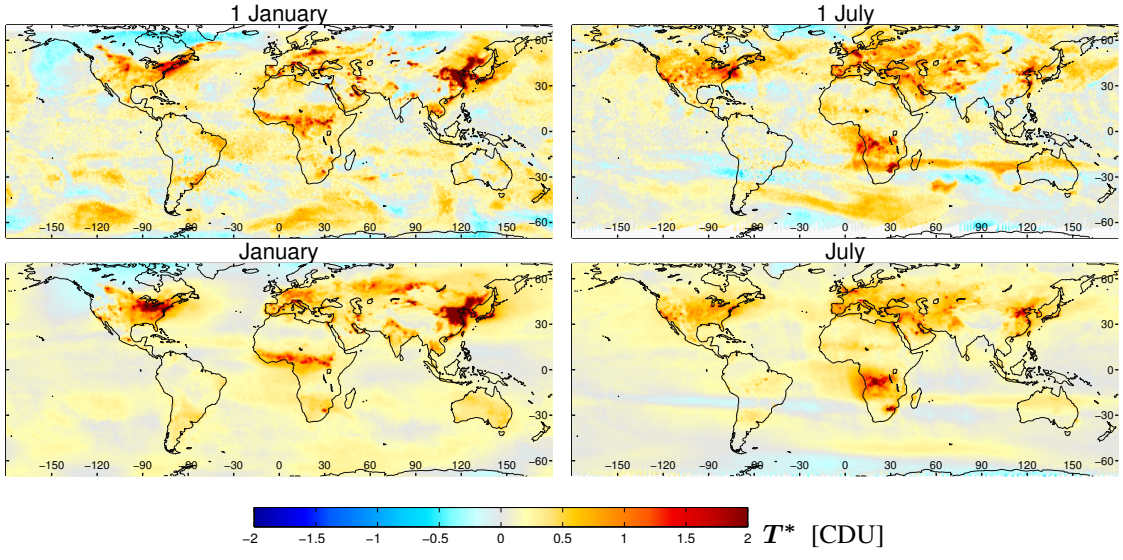

Fig. S 13. OMI tropospheric residues T^* based on STREAM for January (left) and July (right) 2005 for the first day of the month (top) and the monthly mean (bottom) resulting from weighted convolution using G^{eq}.

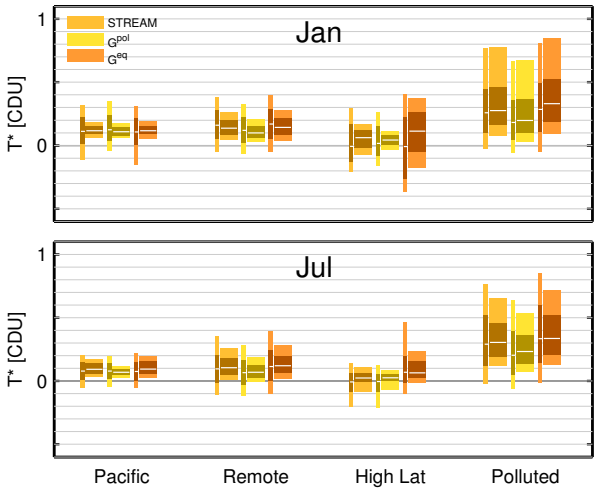

Fig. S 14. Regional statistics of tropospheric residues T^* from STREAM for different settings of the CK G (compare sect. 2.3). Conventions as in Fig. S11.

S4.2.3 Impact of latitude correction

Figure S15 displays the TR resulting from STREAM if the a-priori correction of latitudinal dependency before weighted convolution is switched off for OMI in 2005.

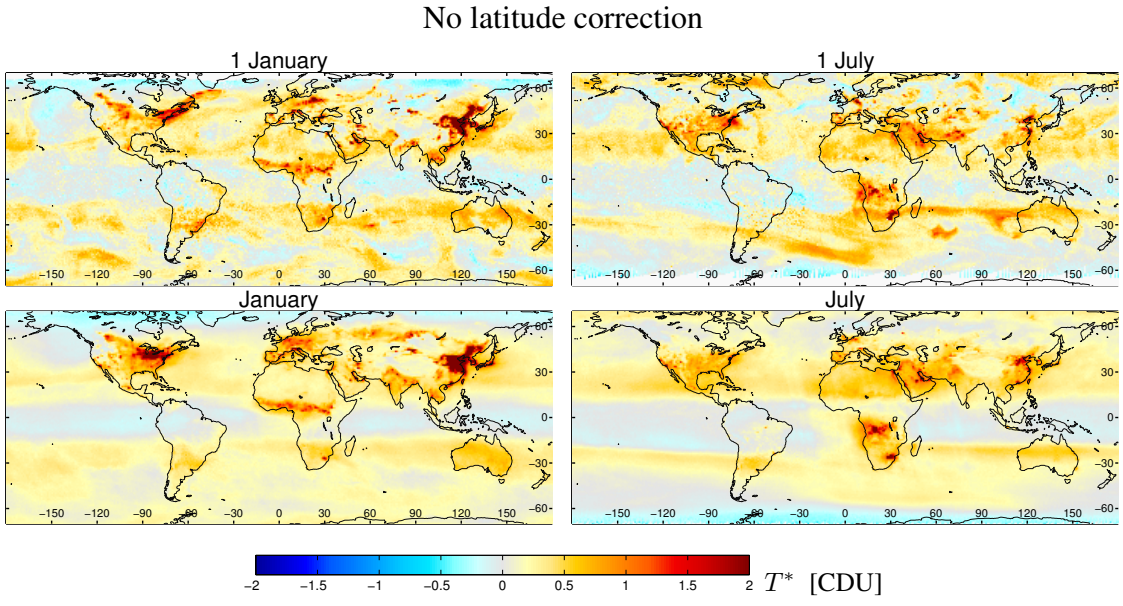

Fig. S 15. OMI tropospheric residues T^* based on STREAM for January (left) and July (right) 2005 for the first day of the month (top) and the monthly mean (bottom) for latitude correction switched off.

S4.2.4 Impact of the number of considered orbits

Figure S16 summarizes the statistics of TR for variations of the number of orbits included for the stratospheric estimate.

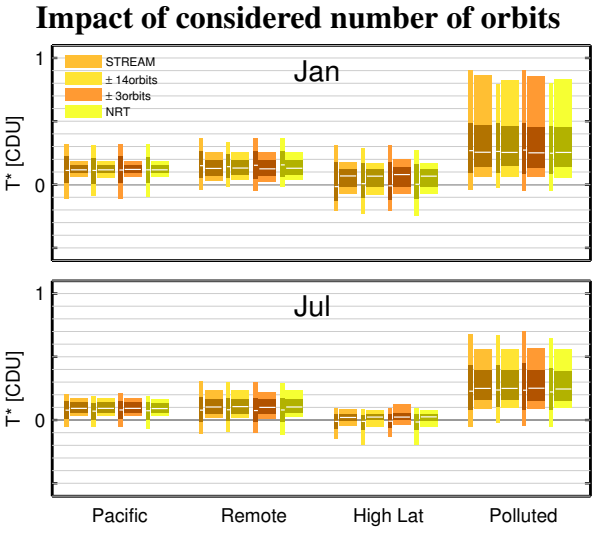

Fig. S 16. Regional statistics of OMI tropospheric residues T^* fromSTREAM for different number of orbits considered in weighted convolution for January (top) and July (bottom) 2005. Conventions as in Fig. S11.

S4.2.5 Impact of tropospheric residue weight

Figure S17 summarizes the statistics of TR for variations of the number of iterations with w_{TR}.

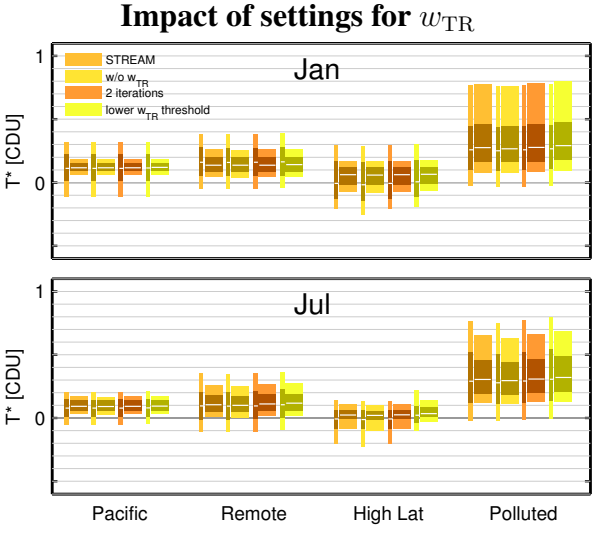

Fig. S 17. Regional statistics of OMI tropospheric residues T^* fromSTREAM for different settings for $w_{\mathrm{TR}}$for January (top) and July (bottom) 2005. Conventions as in Fig. S11.

S4.3 Performance for synthetic data

Figure S18 displays the expected error of T^* , i.e. the difference of estimated and "true" a priori TR, based on synthetic total columns for OMI in 2005.

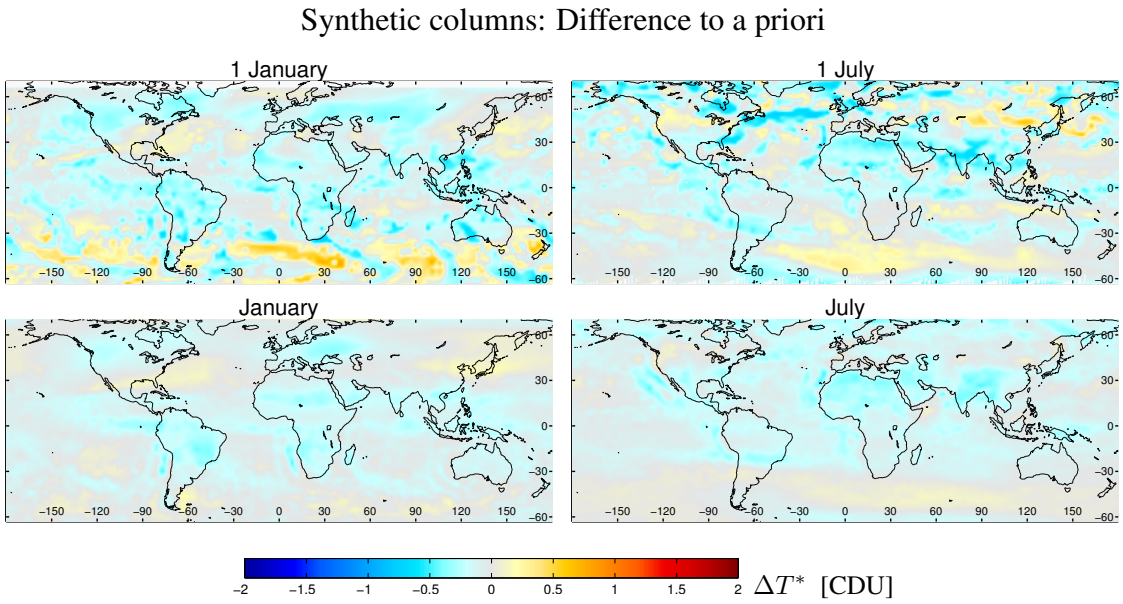

Fig. S 18. Expected error of T^* from STREAM based on synthetic total columns in January (left) and July (right) 2005 for the first day of the month (top) and the monthly mean (bottom).

S5 Discussion

S5.1 OMI

S5.1.1 Comparison to DOMINO

Figure S19 displays the TR resulting from data assimilation as provided in DOMINO for OMI in 2005.

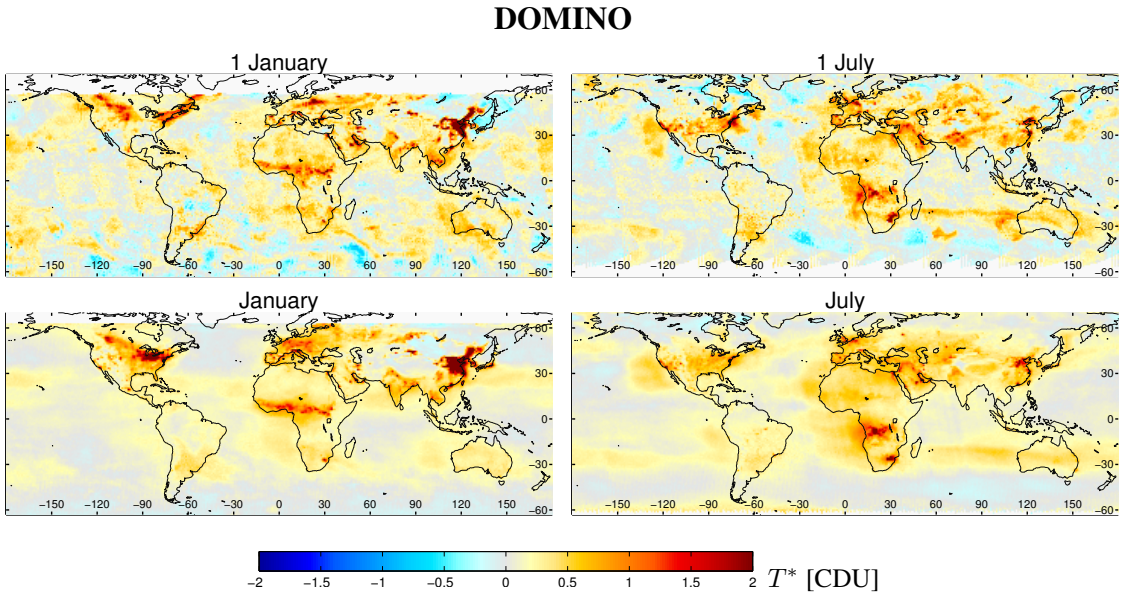

Fig. S 19. OMI tropospheric residues T^* from DOMINO for January (left) and July (right) 2005 for the first day of the month (top) and the monthly mean (bottom).

S5.1.2 Comparison to NASA

Figure S20 displays the TR resulting from NASA v3 for OMI in 2005.
Figures S21 and S22 provide additional case studies of features of the NASA stratospheric estimate (see main text for discussion).

S5.1.3 Comparison to STS EMAC

Figure S23 displays the TR resulting from $\mathrm{STS_{EMAC}}$ for OMI in 2005.

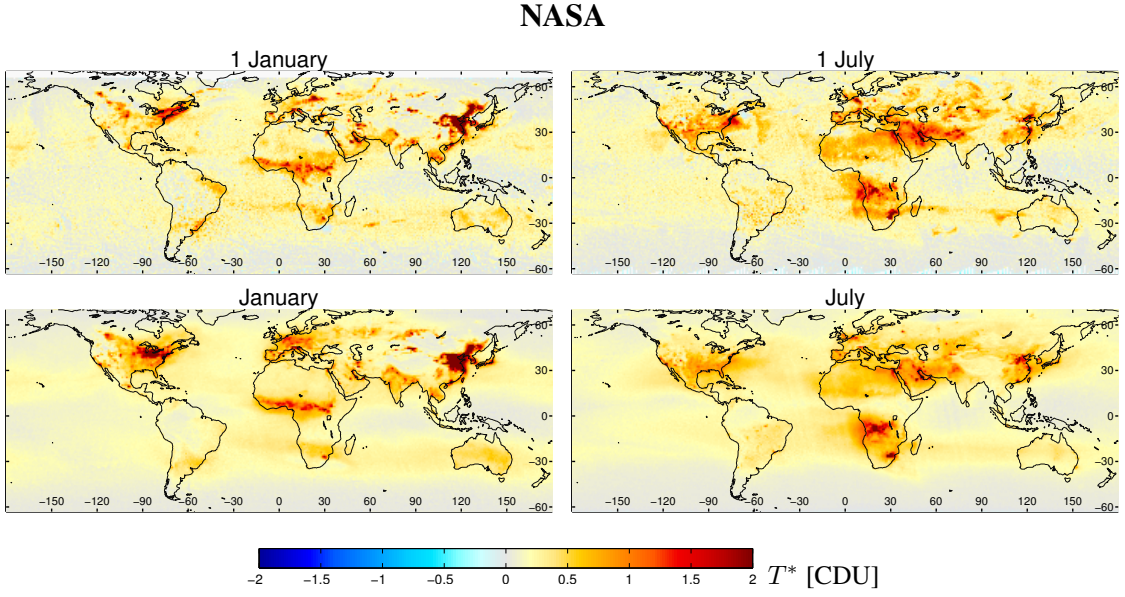

Fig. S 20. OMI tropospheric residues T^* from NASA for January (left) and July (right) 2005 for the first day of the month (top) and the monthly mean (bottom).

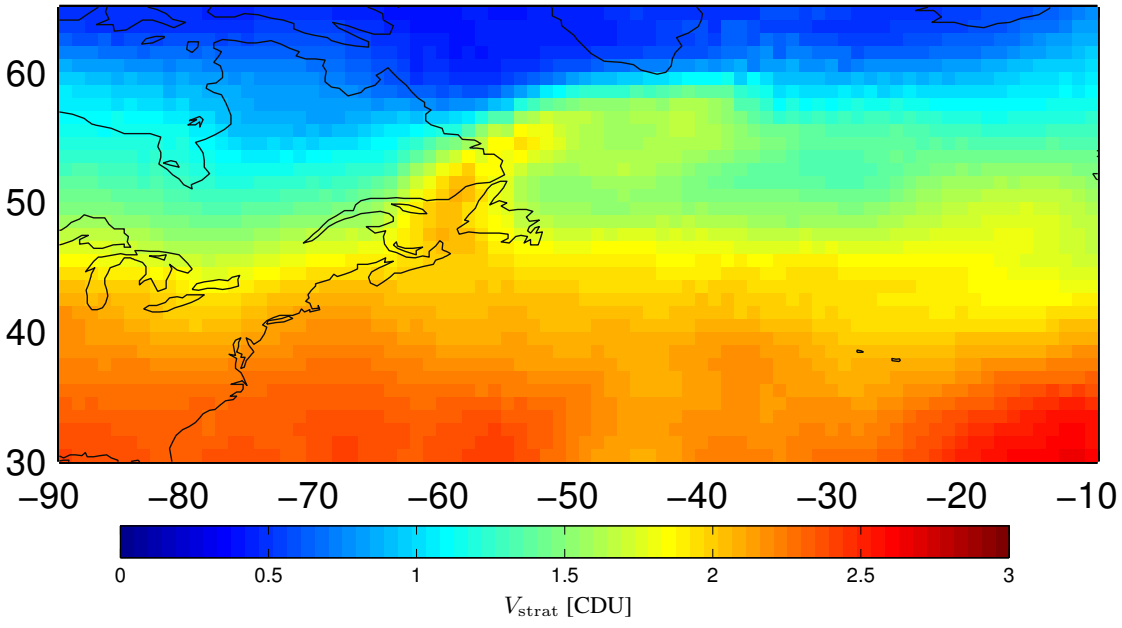

Fig. S 21. Stratospheric VCD as provided by NASA for 1 January 2005. The outflow pattern of NO_2 east of Canada, which is also visible in the total column (Fig. 3 top left), is partly classified as stratospheric.

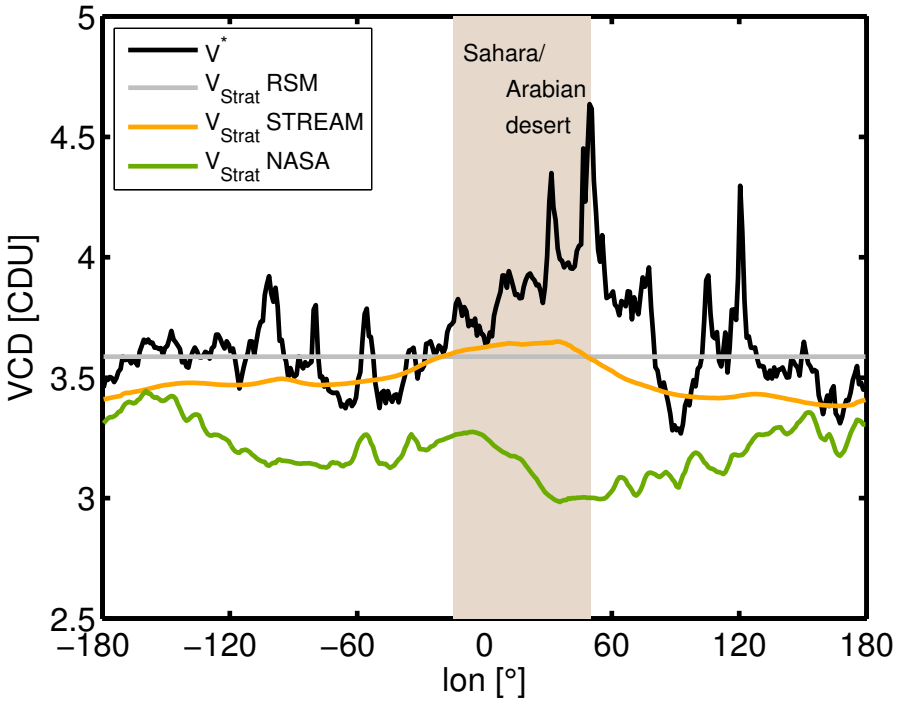

Fig. S 22. Longitudinal dependency of total and stratospheric NO_2 column densities in July 2005 for 20°-30°N. Over the Sahara, V^* as well as V_{strat} from STREAM are maximal, while V_{strat} from NASA (which skips the Sahara for the stratospheric estimation) shows a local minimum.

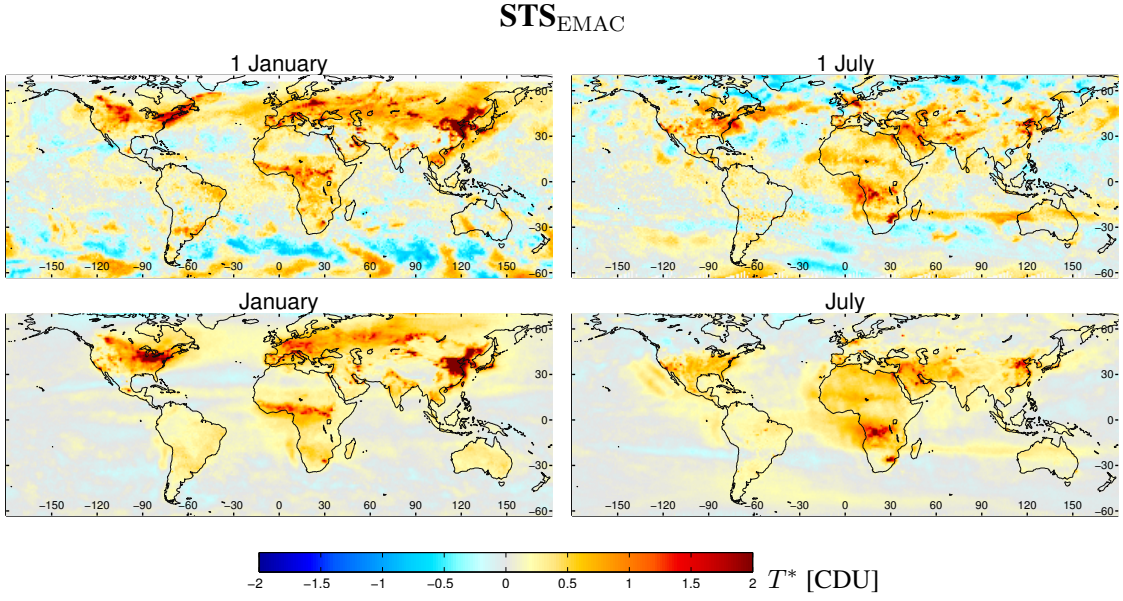

Fig. S 23. OMI tropospheric residues T^* from $\mathrm{STS_{EMAC}}$ for January (left) and July (right) 2005 for the first day of the month (top) and the monthly mean (bottom).

S5.1.4 OMI after row anomaly

Figure S24 displays the TR resulting from STREAM for OMI in 2010, analogue to Fig. 5. Due to the row anomaly, gaps occur in the daily maps. Regional statistics, however, are quite similar to those in 2005 (compare Fig. S25 and Fig. 8).

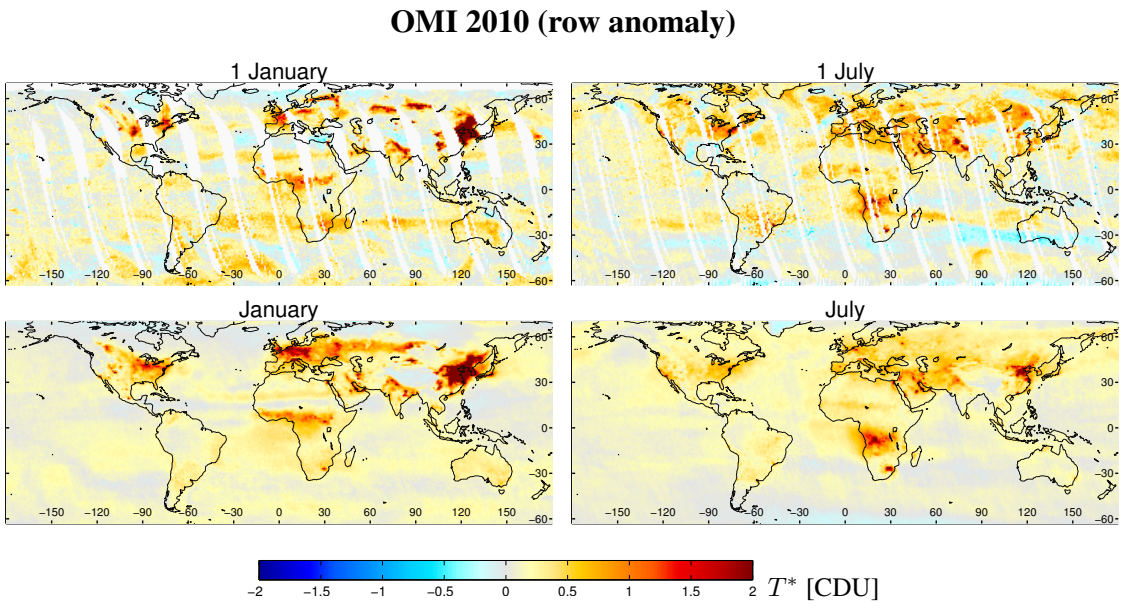

Fig. S 24. OMI tropospheric residues T^* based on STREAM for January (left) and July (right) 2010 for the first day of the month (top) and the monthly mean (bottom).

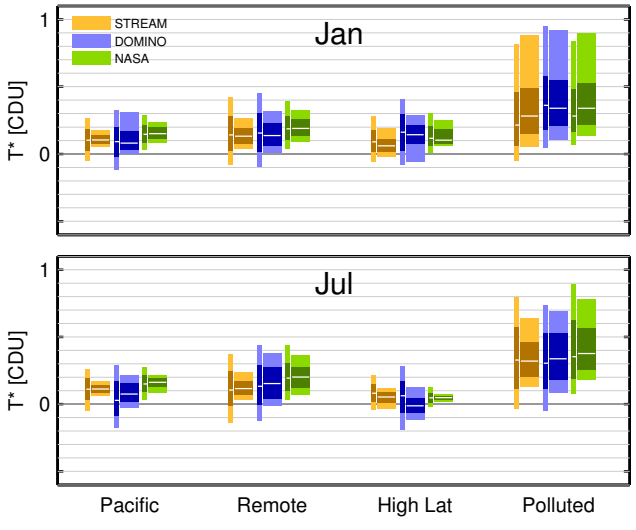

Fig. S 25. Statistics of OMI tropospheric residues T^* from different algorithms for different regions of the globe for January (top) and July (bottom) 2010. Conventions as in Fig. S11.

S5.2 GOME-2

Figure S26 displays the TR resulting from STREAM for GOME-2 in 2010. On 1 July 2010, measurements are performed in narrow swath mode.
Figure S27 shows the artefacts in total and stratospheric VCD caused by a solar eclipse on 15 January 2010. This event was removed from the monthly mean.

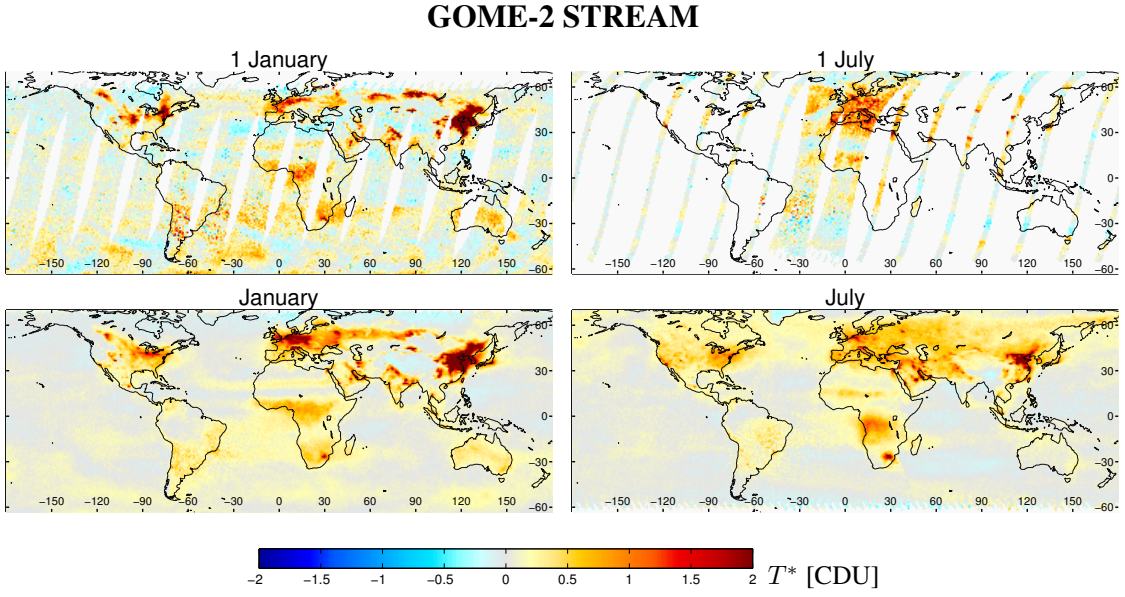

Fig. S 26. GOME-2 tropospheric residues T^* based on STREAM for January (left) and July (right) 2010 for the first day of the month (top) and the monthly mean (bottom).

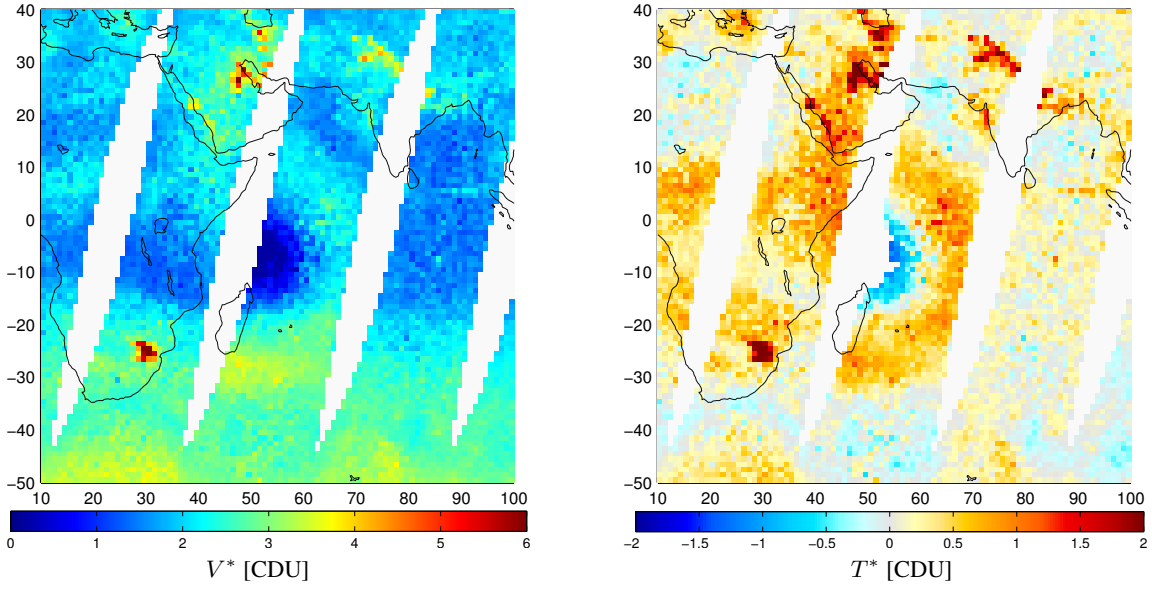

Fig. S 27. GOME-2 total VCD (left) and tropospheric residues T^* (right) on 15 January 2010. Negative VCDs are observed East from Africa caused by a solar eclipse. Thus, T^* shows large artificial patterns.

S5.2.1 Comparison to NRT

Figure S28 displays the TR resulting from STREAM in NRT mode for GOME-2 in 2010.

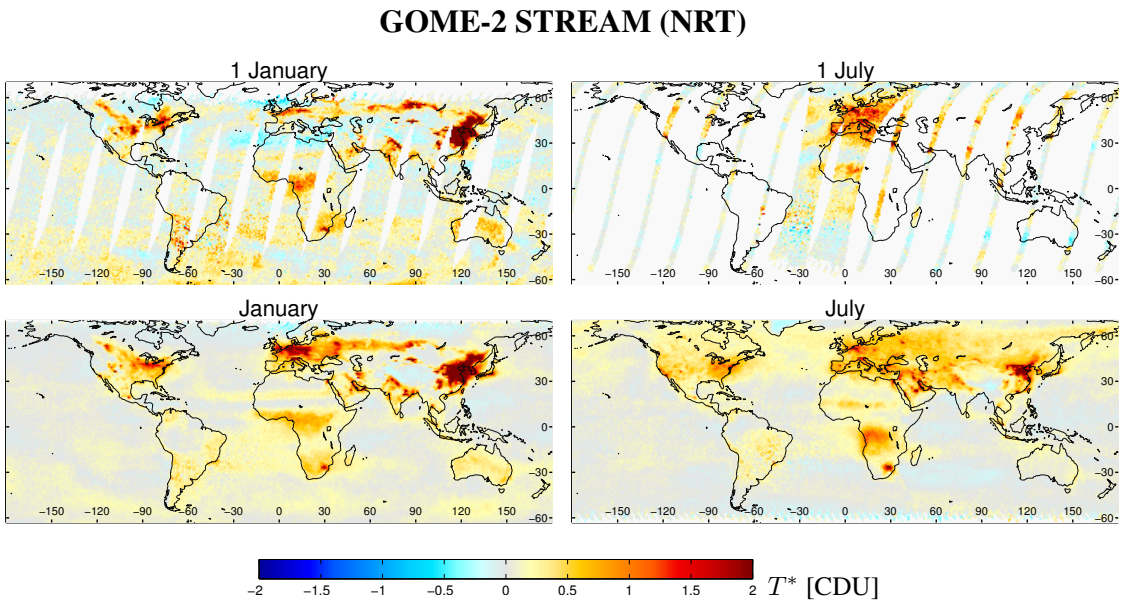

Fig. S 28. GOME-2 tropospheric residues T^* based on STREAM in NRT mode for January (left) and July (right) 2010 for the first day of the month (top) and the monthly mean (bottom).

S5.2.2 Comparison to GDP 4.7

Figure S29 displays the TR resulting from GDP 4.7 for GOME-2 in 2010.

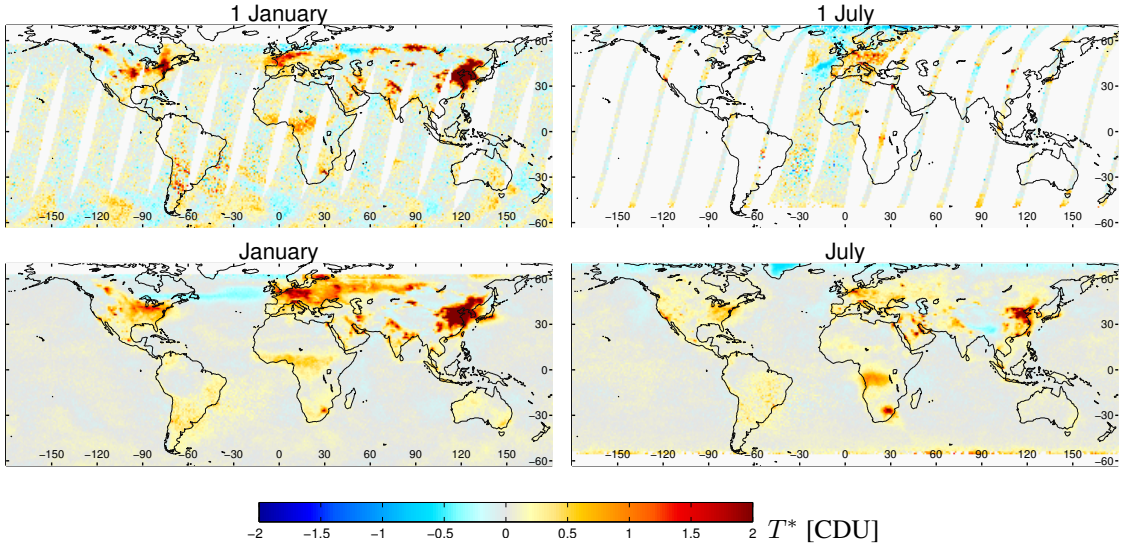

Fig. S 29. GOME-2 tropospheric residues T^* as provided by GDP 4.7 for January (left) and July (right) 2010 for the first day of the month (top) and the monthly mean (bottom).

S5.3 SCIAMACHY

Figure S30 displays the TR resulting from STREAM for SCIAMACHY in 2010.

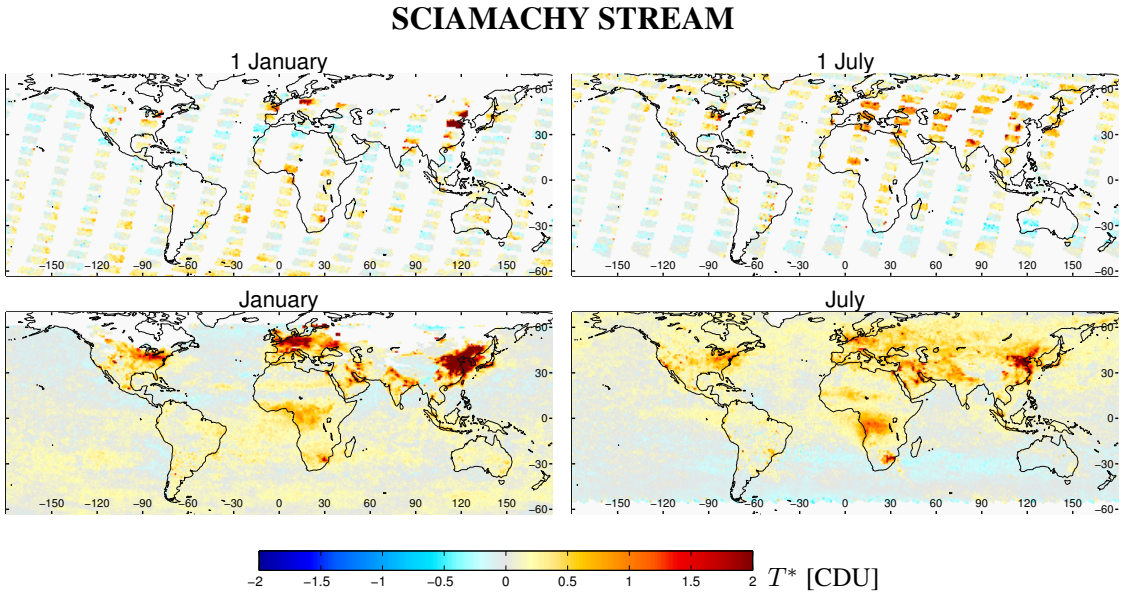

Fig. S 30. SCIAMACHY tropospheric residues T^* based on STREAM for January (left) and July (right) 2010 for the first day of the month (top) and the monthly mean (bottom).

S5.3.1 Comparison to LNM

Figure S31 displays the TR resulting from LNM for SCIAMACHY in 2010.

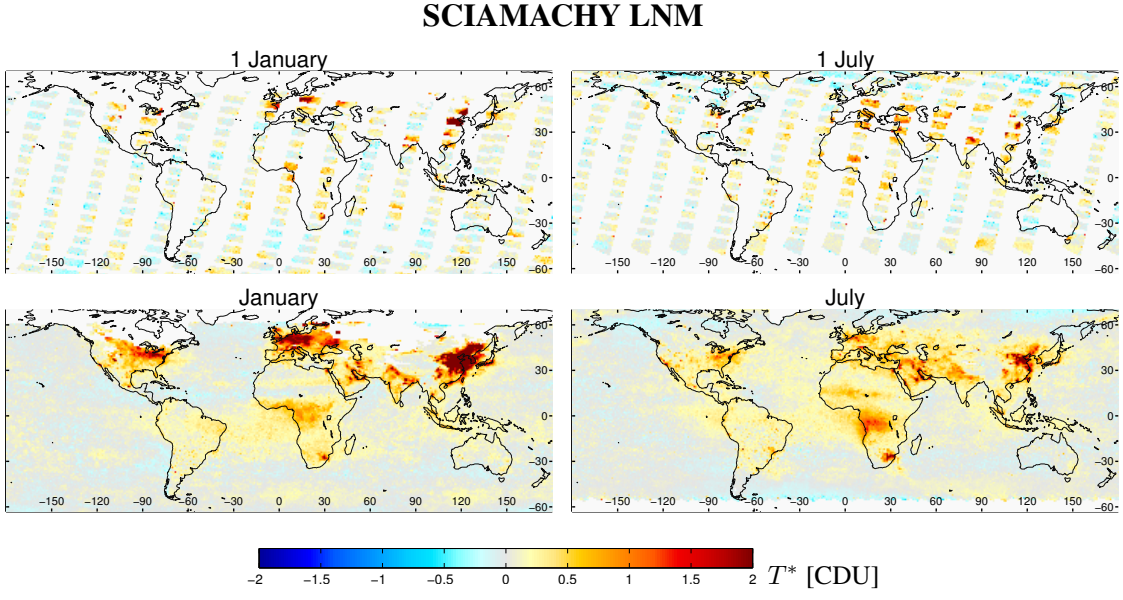

Fig. S 31. SCIAMACHY tropospheric residues T^* based on LNM for January (left) and July (right) 2010 for the first day of the month (top) and the monthly mean (bottom).

Figure S32 displays the mean total VCD V^* over the Pacific as function of latitude, separately for low and high cloud weight. On the summer hemisphere, V^* is lower over clouded pixels, as expected, as the tropospheric background is shielded. This is however not observed in the winter hemisphere, where clouded and cloud free pixels show no difference in V^*, for reasons not yet fully understood. This difference in latitudinal dependency of V^* for clouded vs. cloud free pixels causes the latitudinal dependent biases in the comparison to LNM (Fig. 15).

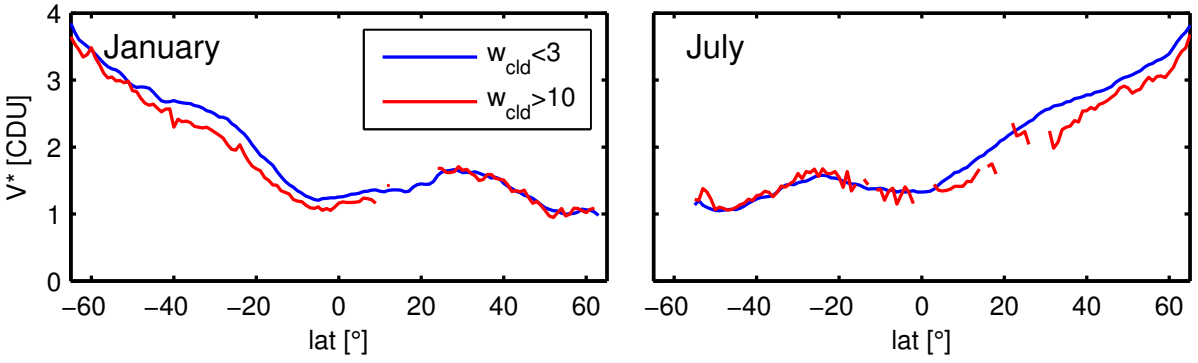

Fig. S 32. Mean V^* over the Pacific as function of latitude, separately for low and high cloud weight, for SCIAMACHY measurements on 1 January (left) and 1 July (right) 2010.

S5.4 GOME

Figure S33 displays the TR resulting from STREAM for GOME in 1999.

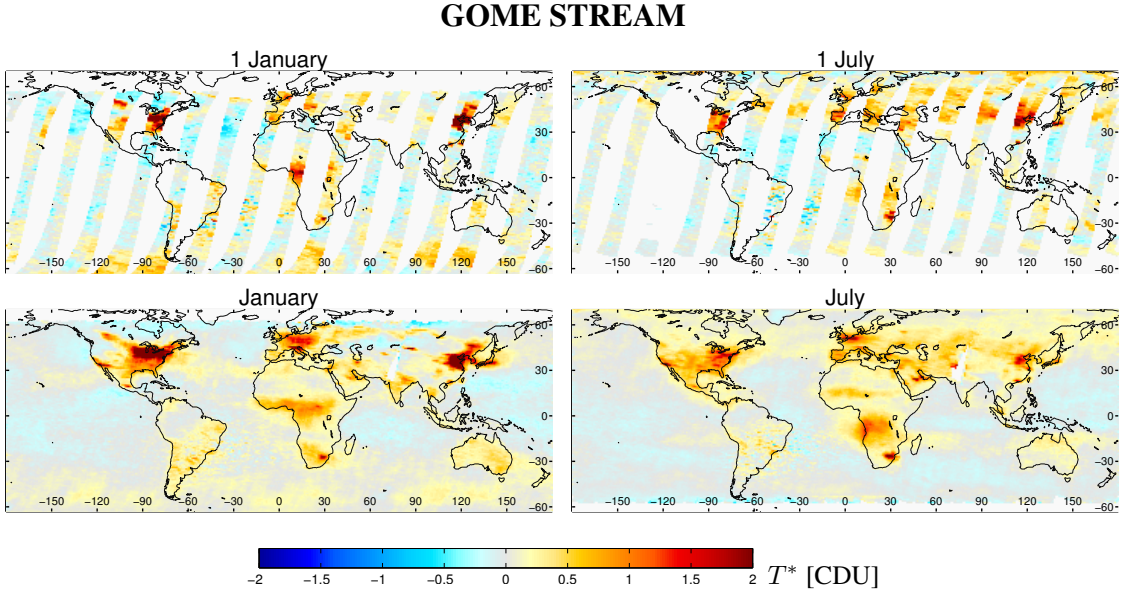

Fig. S 33. GOME tropospheric residues T^* based on STREAM for January (left) and July (right) 1999 for the first day of the month (top) and the monthly mean (bottom).